Journal of Power Sources 260 (2014) 349–356

Contents lists available at ScienceDirect

Journal of Power Sources

journal homepage: www.elsevier.com/locate/jpowsour

N,N′-Bis(salicylidene)ethylenediamine as a nitrogen-rich precursor to synthesize electrocatalysts with high methanol-tolerance for polymer electrolyte membrane fuel cell oxygen reduction reaction

Xuejun Zhou [a], Pan Xu [a], Li Xu [a], Zhengyu Bai [b,*], Zhongwei Chen [c], Jinli Qiao [a,b,*], Jiujun Zhang [b,d]

[a] College of Environmental Science and Engineering, Donghua University, 2999 Ren'min North Road, Shanghai 201620, PR China
[b] School of Chemistry and Chemical Engineering, Henan Normal University, Key Laboratory of Green Chemical Media and Reactions, Ministry of Education, Xinxiang 453007, PR China
[c] Department of Chemical Engineering, E6-2006, University of Waterloo, 200 University Avenue West, Waterloo, ON N2L 3G1, Canada
[d] NRC Energy, Mining & Environment, National Research Council of Canada, 4250 Wesbrook Mall, Vancouver, B.C. V6T 1W5, Canada

HIGHLIGHTS

- Co–N–S/C catalysts for ORR are synthesized using salen as N-ligand by pyrolyzing process.
- The overall electron transfer numbers for the catalyzed ORR are 3.6–3.9 with 3.7–19.9% $\%H_2O_2$ yield.
- The graphitic-N groups are found to be the most active sites for ORR activity.
- These Co–N–S/C catalysts exhibit the superior methanol tolerance to commercial 40% Pt/C.

ARTICLE INFO

Article history:
Received 13 October 2013
Received in revised form
15 February 2014
Accepted 8 March 2014
Available online 15 March 2014

Keywords:
Oxygen reduction reaction
Non-precious metal catalyst
Active sites
Methanol tolerance
Alkaline fuel cell

ABSTRACT

A cost-effective chemical, *N,N′*-bis(salicylidene)ethylenediamine (salen), is used as a ligand to form a carbon-supported Co-salen complex (Co-salen/C) by a simple solid-sate reaction. The Co-salen/C is then pyrolyzed at 600, 700, 800, 900, and 1000 °C to form carbon-supported Co–N–S/C catalysts for the oxygen reduction reaction (ORR). XRD, EDX, TEM, and XPS are used to characterize the catalysts' composition, crystalline nature, morphology, and possible surface groups induced by heat-treatment. Investigation of the catalytic activity and the ORR mechanisms using rotating disk electrode and rotating ring-disk electrode techniques demonstrates that all of these Co–N–S/C catalysts are highly active for the ORR in an O_2-saturated 0.1 M KOH solution, but the catalyst heat treated at 700 °C gives the best ORR activity. The overall electron transfer number for the catalyzed ORR was determined to be 3.6–3.9, with 3.7–19.9% H_2O_2 production over the potential range of −0.05 to −0.60 V, suggesting that the ORR catalyzed by Co–N–S/C catalysts is dominated by a 4-electron transfer pathway from O_2 to H_2O. In addition, these catalysts exhibit superior methanol tolerance to commercial 40% Pt/C catalyst, thus the Co–N–S/C catalysts are promising for use as electrocatalysts in alkaline polymer electrolyte membrane fuel cells.

1. Introduction

In both acidic and alkaline polymer electrolyte membrane (PEM) fuel cells and in metal-air batteries, the catalytic cathode oxygen reduction reaction (ORR) is more challenging than the anode fuel or metal oxidation reactions, because it dominates the devices' performance in terms of both power density and durability [1,2]. In the current state of technology, Pt-based catalysts must be used to catalyze the slow ORR to make PEM fuel cells technically feasible

* Corresponding authors. School of Chemistry and Chemical Engineering, Henan Normal University, Key Laboratory of Green Chemical Media and Reactions, Ministry of Education, Xinxiang 453007, PR China. Tel.: +86 21 67792379; fax: +86 21 67792159.
E-mail addresses: baizhengyu2000@163.com (Z. Bai), zhwchen@uwaterloo.ca (Z. Chen), qiaojl@dhu.edu.cn (J. Qiao), jiujun.zhang@nrc.gc.ca (J. Zhang).

http://dx.doi.org/10.1016/j.jpowsour.2014.03.017
0378-7753/

and practical. However, due to the need for high Pt loadings at fuel cell cathodes, and Pt catalysts' low fuel tolerance (e.g., in direct alcohol fuel cells) [3,4], it is advisable to replace Pt with non-precious metal catalysts [5].

In recent years, alkaline PEM fuel cells have been recognized as feasible energy conversion devices for several reasons [6–8]. One of their major advantages is the possible usage of non-noble metal catalysts for the ORR. These catalysts are cost-effective and at the same time fuel tolerant. In a direct alcohol fuel cell, for example, due to unavoidable fuel crossover from anode to cathode, it is highly desirable that the cathode catalyst not have catalytic activity towards the fuel. If the cathode catalyst is catalytically active toward fuel oxidation (meaning it has no fuel tolerance), either the cathodic O_2 reduction potential of the corresponding fuel cell will be depressed or the fuel efficiency will be reduced. Using alkaline PEM fuel cells, this issue of fuel crossover can be lessened. This is because the conduction ion in an alkaline PEM fuel cell membrane (the anion exchange membrane) is OH^-, which transfers from cathode to anode during operation – in the opposite direction of fuel crossover, which proceeds from anode to cathode – leading to much less fuel crossover than in acidic PEM fuel cells, where the direction of proton transfer is the same as that of fuel crossover [6]. Therefore, using an alkaline PEM fuel cell catalyzed by a fuel-tolerant cathode catalyst will be highly beneficial to fuel cell performance and fuel efficiency.

In fact, since Jasinski first observed that cobalt phthalocyanine could catalyze the ORR in an alkaline medium [9], intensive research has been conducted to explore transition metal macrocycles as cathode catalysts for the ORR. However, poor stability is their major disadvantage. It was reported that the stability can be greatly improved by using heat-treatment procedures. The enhancement can be attributed to lower production of hydrogen peroxide, which is capable of oxidizing and splitting the active sites. Although significant progress has been achieved with heat-treated macrocyclic compounds as ORR catalysts, the activity and stability of such catalysts are still insufficient to replace Pt at the fuel cell cathode. Moreover, transition metal macrocycles are still expensive because their synthesis is complex. A significant breakthrough was made by Yeager et al. [10], who demonstrated that expensive macrocycles could be substituted by individual metal and N precursors. Since then, many simple and cost-effective nitrogen-containing ligands for metal-complex catalysts have been explored, such as polypyrrole [11,12], ethylene diamine [13], cyanamide [14], and phenanthroline [15]. Although the nature of the active ORR catalytic sites in such M–N–C catalysts is still not entirely understood, it is widely accepted that the ORR performance of these catalysts strongly depends on the type of nitrogen and transition-metal precursors used, the heat-treatment temperature, the carbon support, and the synthesis conditions [16,17]. Therefore, further exploring new materials and optimizing catalyst synthesis conditions to achieve highly active and stable non-precious metal catalysts is definitely necessary [18].

Most recently, using pyridine as a nitrogen-rich ligand and cobalt sulfate heptahydrate as a metal precursor, we synthesized carbon-supported Co-nitrogen catalysts (CoPy/C) that are highly active for the ORR after high-temperature treatment [19]. These synthetic catalysts thus offer tremendous potential for achieving better functionality than Pt by manipulating the catalysts' active components. In a continuation of this effort, we here demonstrate that *N*,*N*′-bis(salicylidene)-ethylenediamine (salen), as a new promoter, can significantly enhance the electrocatalytic activity of the Co site, due to the formation of carbon-supported Co–N–S catalysts after heat-treatment. Unlike pyridine, salen contains two nitrogen atoms that can form a chelate structure with metal Co, thereby making the active sites more available, even though the relative nitrogen content of Co-salen is lower than that of Co-pyridine. We used several instrumentation methods–powder X-ray diffraction (XRD), transmission electron microscopy (TEM), energy dispersive X-ray (EDX) spectroscopy, as well as X-ray photoelectron spectroscopy (XPS) – to characterize the structure and composition of the catalysts and thereby obtain insight into their ORR catalytic activity and its dependence on heat-treatment temperature. The reaction kinetics and mechanism of the ORR on these materials were analyzed in oxygen-saturated alkaline solutions by cyclic voltammetry (CV) and rotating disk electrode (RDE) techniques as well as rotating ring-disk electrode (RRDE) measurements. The ORR catalyzed by Co–N–S/C catalysts in the presence of methanol was also studied and compared with commercially available Pt/C to evaluate the applicability of Co–N–S/C in direct methanol alkaline fuel cells.

2. Experimental

2.1. Materials and catalyst synthesis

For catalyst synthesis, the following starting materials were used: *N*,*N*′-bis(salicylidene)ethylenediamine (salen) (analytic grade, Aldrich), cobalt sulfate heptahydrate ($CoSO_4{\cdot}7H_2O$) (analytic grade, Aldrich), methanol (analytic grade, Aldrich), and Vulcan XC72R carbon black (Cabot Corporation, $S_{BET} = 236.8\ m^2\ g^{-1}$). All of these materials were used without further purification. The catalysts in this study were synthesized using a solid-state reaction. In a typical synthesis, a mixture of 0.143 g $CoSO_4\ 7H_2O$, 0.075 g salen, and 0.180 g XC72R carbon black were mixed with 20 ml methanol, carefully milled for about 2 h in a mortar, and then vacuum dried at 40 °C for 1 h. In this process, a chemical reaction between Co(II) ion and salen ligand occurred on the carbon particles, forming carbon-supported Co(II)-salen complex (abbreviated as Co-salen/C). This powder was then placed in a crystal boat and heat treated at 600, 700, 800, 900, and 1000 °C, in each instance for 2 h under N_2 atmosphere. Analysis using XRD, EDX, and XPS showed that the catalysts formed after heat-treatment contained Co, C, N, S, and O, thus we denote these catalysts as Co–N–S/C-*T*, where *T* is the heat-treatment temperature.

2.2. Instrument characterizations

The crystallinity of the various catalyst samples was determined by XRD using a Rigaku D/max-2550 V diffractometer with Cu Kα radiation operating at 30 kV and 40 mA. TEM analyses were performed on a high-resolution Hitachi JEM-2100 system operating at 200 kV. The catalyst bulk composition was verified by means of EDX. Surface analysis of the catalyst particles was carried out by XPS on an RBD-upgraded PHI-5000C ECSA system (PerkinElmer) with an Al K X-ray anode source ($h\nu = 1486.6$ eV) at 14.0 kV and 250 W.

2.3. Electrochemical measurements

The catalysts' performance for the ORR was measured in a thermostat-controlled, standard three-electrode cell at room temperature with a Pt-wire counter electrode, a saturated calomel electrode (SCE) reference electrode, and a rotating glassy carbon (GC) disk electrode as the working electrode. For catalyst-layer preparation on the working electrode surface, please refer to our recent publication [19]. Prior to the ORR experiments, the electrolyte was deaerated by bubbling with N_2 for at least 30 min. Steady cyclic voltammograms were obtained at a scan rate of 50 mV s^{-1} within an electrode potential range of −0.3 to 0.8 V vs. standard hydrogen electrode (SHE). For the ORR measurements using a RDE,

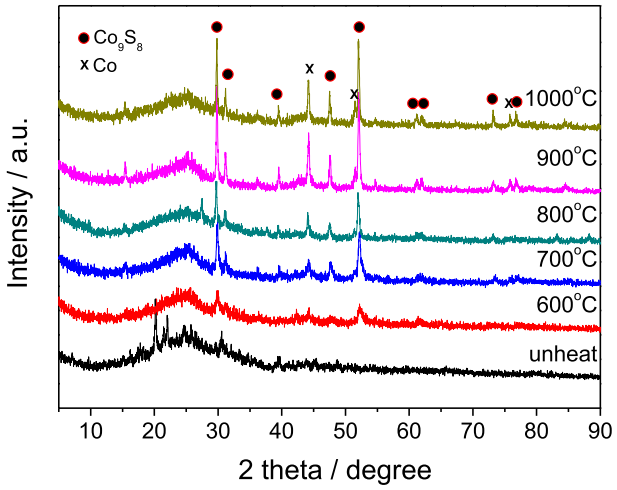

Fig. 1. XRD patterns for catalysts before and after heat treatment at different temperatures.

the Co-salen/C or Co–N–S/C-*T* coated GC electrode was rotated at speeds from 300 to 2400 rpm in O_2-saturated 0.1 M KOH solution, and the RDE current–voltage curves were recorded at a potential scan rate of 5 mV s^{-1}. For measurements using RRDE, which were used to detect the H_2O_2 produced during the catalyzed ORR, the same conditions as in the RDE experiments were used, with an electrode containing a Pt ring (6.25 mm inner diameter and 7.92 mm outer diameter) and a GC disk (5.61 mm diameter) employed as the working electrode. The catalyst ink was prepared in the same way as for the RDEs. An amount of ink was loaded on the GC rotating disk electrode to keep the same catalyst loading as in the RDE measurements. A potential of 1.20 V vs. reversible hydrogen electrode (RHE) was applied to the Pt ring electrode, which had a collection efficiency of 0.37. All measured potentials vs. SCE in this work were converted to SHE, as shown in the relevant text and figures.

3. Results and discussion

3.1. Physical characterization of the catalysts' composition, structure, and morphology

Fig. 1 shows XRD patterns that elucidate the crystallographic nature of Co-salen/C and Co–N–S/C catalysts prepared at 600, 700, 800, 900, and 1000 °C, respectively. As shown in Fig. 1, the broad signals centered at 24.7° can be assigned to the (002) diffraction peak of graphitic carbon. As expected, for Co-salen/C catalyst, there is no indication of metallic Co. However, when the sample was heat treated, two crystalline peaks at 44.3° and 51.6° were observable, although their peak magnitudes are not obvious at 600 °C. These two peaks are ascribed to metallic Co aggregation [20,21], indicating that part of the Co-salen on the carbon support may have decomposed to produce metallic Co and the new composition of Co–Nx–C. As the temperature increases from 600 to 1000 °C, the magnitudes of these two peaks significantly increase, suggesting the growth of metallic Co particles after decomposition of the Co-salen structure. Other peaks, such as at 30°, 31.2°, 47.5°, and 51.9°, can be assigned to Co_9S_8 [22]. The S in Co_9S_8 should have come from the SO_4^{2-} anion in $CoSO_4$, as was also observed for CoPy/C catalyst in our recent paper [19].

Fig. 2 displays typical TEM images of Co-salen/C and Co–N–S/C catalysts prepared at 600, 700, and 1000 °C, respectively, to investigate particle size distribution. The carbon black particles have an amorphous structure with particle sizes of 20–30 nm and are covered by Co-salen complex (Fig. 2(a), with dark contrast). After heat treatment at 600 °C, the aggregate size of the Co-salen complex on the carbon support surface decreases, and small metal particles without a clear shape form (Fig. 2(b)). However, metal particles surrounded by graphitic carbon shells with an average particle size of ~10 nm can be clearly observed after heat treatment at 700 °C (Fig. 2(c)), suggesting that the Co-salen complex decomposed. For the catalyst sample further heat treated at 1000 °C, the mean particle sizes increase sharply to 80–100 nm (Fig. 2(d)). These results suggest that heat treatment can decompose the Co-salen complex to metallic Co, which then agglomerates

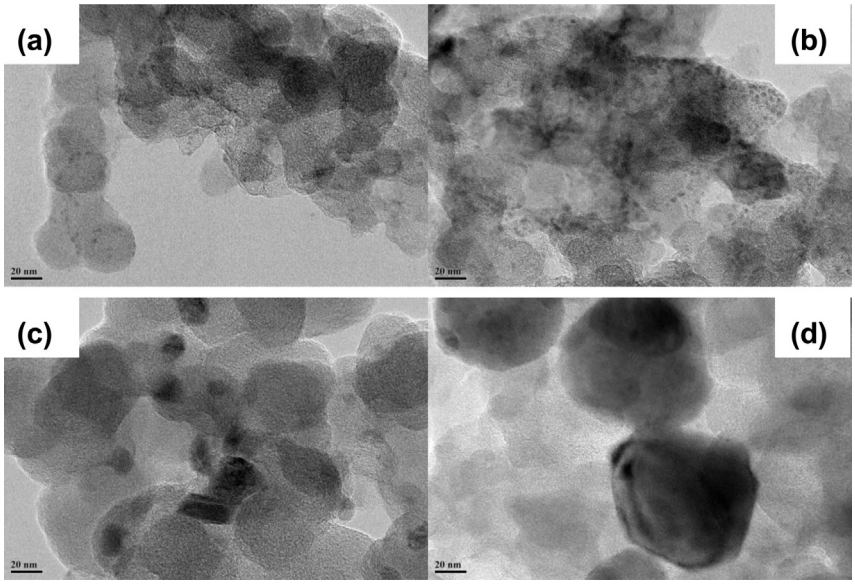

Fig. 2. TEM images of (a) Co(salen)/C, (b) Co–N–S/C-600, (c) Co–N–S/C-700, and (d) Co–N–S/C-1000.

Table 1
Elemental quantification analysis of Co–S–N/C-based catalysts with different heat-treatment temperatures.

Catalyst sample	Atomic concentrations, %				
	C	O	N	Co	S
Co-salen/C	81.42	10.16	3.94	2.57	1.89
Co–N–S/C-600	86.14	2.19	2.32	6.07	3.28
Co–N–S/C-700	86.79	1.91	1.90	6.38	3.01
Co–N–S/C-800	87.18	1.55	1.65	6.66	2.96
Co–N–S/C-900	87.05	1.57	1.27	7.04	3.07
Co–N–S/C-1000	87.14	0.86	0.74	8.03	3.23

to form large particle sizes when the temperature further increases. All the above results are in good agreement with the observations from the XRD analysis in Fig. 1.

To determine the elemental composition of Co-salen/C and Co–N–S/C catalysts prepared at different temperatures, EDX analysis was performed, and the results are summarized in Table 1. As detailed there, all catalyst samples consist of Co, C, O, N, and S. Increasing the heat-treatment temperature results in increased Co and C content and a decrease in both N and O content. For example, the N content decreases from 3.94 at% for Co-salen/C to 0.74 at% for Co–N–S/C-1000. This decrease in N content is mainly due to the decomposition of salen, whereas Co species are more stable at high temperatures, so the Co content increases. These results have also been observed by other groups [23,24]. Note that although the N content of Co-salen/C is the highest among all the samples (Table 1), the Co-salen/C catalyst shows the lowest catalytic ORR activity. The explanation could be that these N atoms are not involved in the formation of active sites. Only when the complex is pyrolyzed, some of the N would be converted into the portion of the active sites, as will be discussed in the following section.

An interesting result is that S was detected in both Co-salen/C and Co–N–S/C catalysts prepared at different temperatures, and the S contents in Co–N–S/C-900 (3.07 at%) and Co–N–S/C-1000 (3.23 at%) are much higher than in Co-salen/C (1.89 at%). Analysis of XRD patterns indicates that S is mostly in the form of Co_9S_8 (Fig. 1), which is also believed to be favorable for the ORR, since the catalyst porosity is highly improved [19]. That is why we observed an even higher ORR activity for Co–N–S/C-900 and Co–N–S/C-1000 than for Co–N–S/C-600 and Co-salen/C. This is also further discussed below.

To obtain more detailed information on the elemental oxidation state of the catalysts, XPS measurements were performed. A broad scan of all the samples showed peaks associated with C, N, O, Co, and S (Fig. 3(a)), which is in good agreement with the EDX analysis,

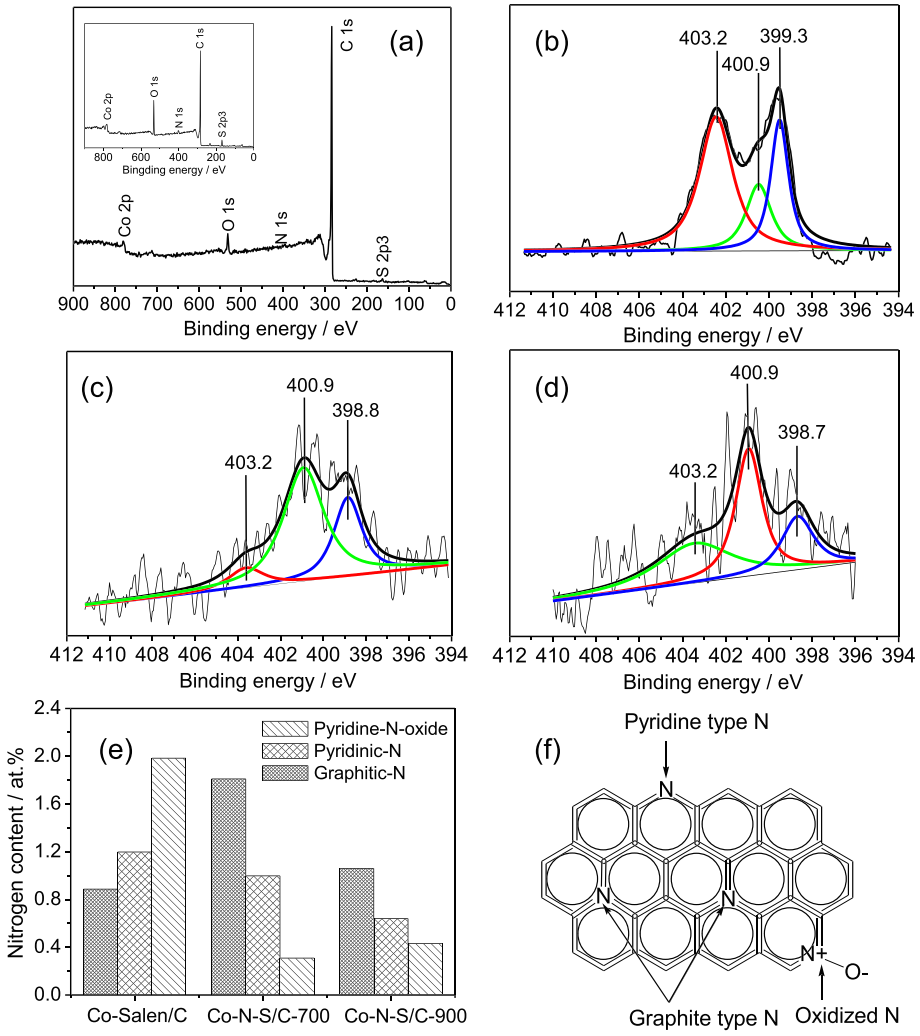

Fig. 3. XPS spectra for (a) Co–N–S/C-700, with insert showing spectra for Co-salen/C; N 1s XPS spectra for (b) Co(salen)/C, (c) Co–N–S/C-700, and (d) Co–N–S/C-900; (e) the content of three nitrogen types; (f) schematic of the bonding configurations of three types of N functionalities.

as shown in Table 1. As nitrogen doping into the carbon structure is likely to play a significant role in ORR catalytic activity, the N 1s spectra for three typical catalyst samples: Co-salen/C (Fig. 3(b)), and Co–N–S/C prepared at 700 °C (Fig. 3(c)) and 900 °C (Fig. 3(d)) were selected as the target materials. We found the surface nitrogen concentrations to be 4.07, 3.12, and 2.13 at% for Co-salen/C, Co–N–S/C-700, and Co–N–S/C-900, respectively. Compared to the values listed in Table 1, the N content is significantly different. This is because the XPS data only reflects the composition within 10 nm of the sample's surface layer, whereas the EDX data listed in Table 1 are for bulk composition. The N content measured by XPS is larger, indicating that the N stays inside the sample's surface layer rather than spreading throughout the bulk of the catalyst. The high-resolution N 1s spectra of all three samples are fitted using three components: pyridinic (~398.8 eV), graphitic (~400.9 eV), and pyridine-N-oxide (~403.6 eV) nitrogen species [25–27]. The amounts of these three types of nitrogen in the catalysts are shown in Fig. 3(e), and the schematic structures are displayed in Fig. 3(f). One can see that for non-pyrolyzed Co-salen/C, pyridine-N-oxide accounts for the greatest part, up to 50%. This type of nitrogen species is believed to make no contribution to ORR performance [28]. In Co–N–S/C-700, the pyridine-N-oxide content decreases dramatically, while pyridinic N and graphitic N comprise around 90% of the nitrogen, with pyridinic N decreasing slightly compared to in Co-salen/C. It has been thought that both pyridinic and graphitic N have some potential to form Co–N_x groups for ORR active sites; indeed, Co–N_x groups have been widely recognized in the literature as ORR active sites. However, in the present study, the pyridinic N contents in the catalysts did not differ significantly, indicating that it may not play an important role in ORR performance. In contrast, graphitic N was increased to 1.81 at% for Co–N–S/C-700, accounting for about 65% of the nitrogen. For Co–N–S/C-900, graphitic N content was decreased to 1.06 at% but still accounted for about 60% of the nitrogen, whereas the pyridinic N content was further decreased to 20% of the nitrogen. As we will discuss later, this trend agrees very well with the trend in the catalysts' ORR activities, suggesting that graphitic N may act as the ORR active site and contribute to higher catalytic activity.

Fig. 4(a) shows the measured Co 2p spectra of the samples. For the non heat-treated catalysts, the Co 2p photoemission peak shows a single Co 2p chemical state at 782.1 eV, and this can be ascribed to Co $2p_{3/2}$ signal of Co in an oxidized Co^{2+} state [29]. After the heat treatment at 700 °C, the peak shifted to lower binding energy, similar to the metallic Co at 780.4 eV, indicating a reduction in the Co species during the process [30–32]. Meanwhile, a new peak appears around 778.2 eV. This can be assumed to be due to the decomposition of the initial complex to form Co–N_x. And this was also observed for the case of pyrolyzed metal macrocyclic compounds [21]. For the sample heat-treated at 900 °C, the intensity of the peak at 778.2 eV decreases, which suggests that the structure of Co–N_x has been destroyed. The above results indicate that Co–N_x bonding is stable below the temperature 700 °C but starts to decompose above this temperature. Considering the results of LSV and RRDE, which show maximum catalytic performances at 700 °C and a subsequent decrease at 900 °C, the Co–N_x can be assumed to be the essential features for the ORR activities. This result is consistent with the previous reports [33,34].

Fig. 4(b) shows the obtained XPS spectra for S_{2p} at a typical heat-treatment temperature of 700 °C. There are basically four peaks, at 162.4, 164.1, 165.0, and 169.2 eV, respectively. According to the literature, the peak at 162.4 eV can be assigned to Co_9S_8 (as observed by XRD, above) [35], the peak at 164.1 eV to S_2^{2-} [36], the peak at 165.0 eV to sulfoxide [37], and the peak at 169.2 eV to sulfur [38]. Both S_2^{2-} and sulfur are soluble in water, so it is impossible for them to be the surface ORR active sites. Therefore, both sulfoxide and Co_9S_8 may have the ability to participate in the ORR process, promoting the ORR activity of the catalysts. This promotional effect was also demonstrated in our previous publication, when CoPy/C was used as the cathode catalyst for the ORR [19]. However, the promotion mechanism is still not clear. More detailed work is definitely needed to understand the role of S in these catalysts.

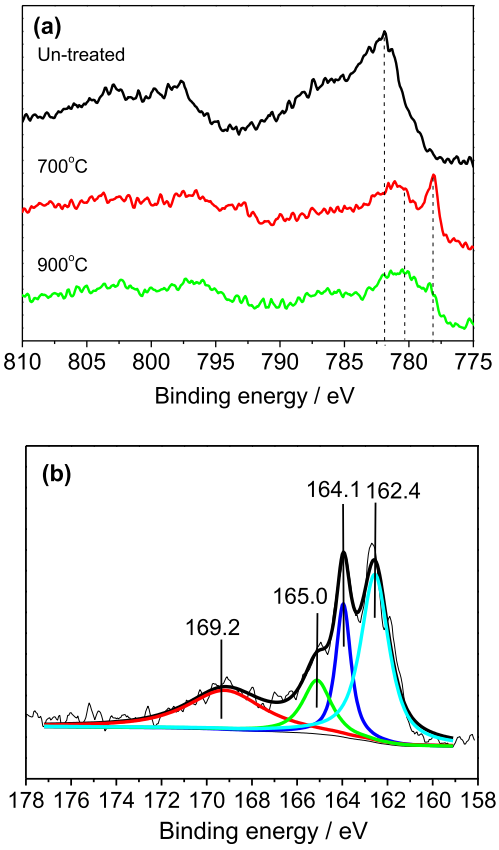

Fig. 4. XPS spectra for (a) Co 2p (b) S 2p for Co–N–S/C-700.

3.2. Electrochemical characterization of the catalysts' surface activity and ORR activity

To assess the ORR catalytic activity of the catalysts, cyclic voltammograms were collected in O_2 vs. N_2-saturated 0.1 M KOH solution using a GC electrode coated with catalysts synthesized at different heat-treatment temperatures. Fig. 5 shows the cyclic

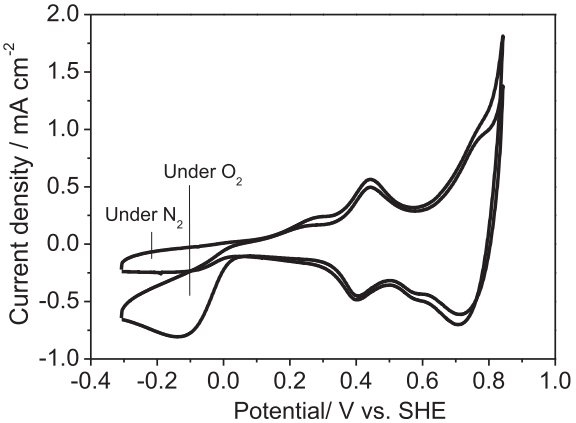

Fig. 5. Cyclic voltammograms of Co–N–S/C-700 at a scan of 50 mV s^{-1} in N_2- or O_2-saturated 0.1 M KOH solution; catalyst loading: 70.6 μg cm^{-2}.

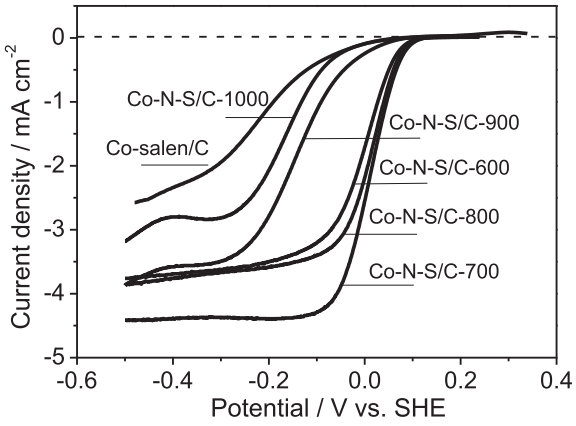

Fig. 6. Polarization curves on rotating disk electrode for Co-salen/C-based catalysts at a scan rate of 5 mV s^{-1} in O_2-saturated 0.1 M KOH solution; catalyst loading: 70.6 μg cm^{-2}; rotation rate: 1500 rpm.

voltammograms profiles of a typical candidate, the catalyst heat treated at 700 °C—i.e., Co—N—S/C-700. In the case of an N_2-saturated 0.1 M KOH electrolyte, two paired peaks at around 0.4 V and 0.7 V are associated with the redox reaction of the cobalt species. (For a more detailed explanation, please refer to our previous publication [17].) In contrast, a well-defined cathodic current appears with a peak centered at about −0.15 V, corresponding to when the electrolyte was saturated with O_2 and indicating high ORR catalytic activity.

To further confirm that heat-treatment temperature enhances catalytic performance for the ORR, Fig. 6 displays the ORR polarization curves for catalysts at various temperatures from 600 to 1000 °C in O_2-saturated 0.1 M KOH solution, with an unheated catalyst sample (Co-salen/C) for comparison. The kinetic parameters for the ORR on Co—S—N/C catalysts with different heat-treatment temperatures are summarized in Table 2. Clearly, the non-treated catalyst exhibits the lowest catalytic activity towards the ORR, based on both the onset potential and the current density, indicating that the heat-treatment temperature has an obvious effect on the catalysts' ORR activity. When the heat-treatment temperature is increased, the catalytic activity largely improves from 600 to 800 °C; the catalyst obtained by heat treatment at 700 °C shows the highest ORR activity among those studied. As shown in Table 2, the ORR half-wave potential for Co—N—S/C-700, $\Delta E_{1/2}$, is 0.02 V, which is a positive shift of ~240 mV compared to Co-salen/C. In addition, the maximum current density for Co—N—S/C-700 is twice that of Co-salen/C, accompanied by a well-defined diffusion limiting current plateau in the potential range below −0.1 V. This further suggests that ~700 °C may be the optimal heat-treatment temperature for obtaining the most electroactive catalyst. Above 800 °C (such as at 900 °C and at 1000 °C), the ORR activity falls drastically but is still much higher than without heat-treatment, i.e., for Co-salen/C. According to the literature, two possible active sites—Co—N_4 or Co—N_2 − bonded on C (i.e., Co—N_x—C moieties) might form on the catalyst surface during the heat-treatment process [31,32]. However, when the temperature is further increased, for example, above 800 °C, part of the Co—N_x ($x = 2$ and/or 4) may decompose to form ORR inactive Co metal or Co oxide, as indicated by XRD and TEM results, thereby reducing the ORR catalytic activity [39,40]. Furthermore, the trend in ORR activity is consistent with the order of graphitic N content, further suggesting that both pyridinic and graphitic N might play an important role in the catalyzed ORR process, but the latter seems dominant.

Table 2
Kinetic parameters for the ORR on Co—S—N/C-based catalysts with different heat-treatment temperatures.

Catalyst sample	Onset potential (V)[a]	$E_{1/2}$ (V)[a]	j_k at −0.10 V (mA cm^{-2})[a]	n at −0.3 V
Co-salen/C	0.06	−0.22	0.47	3.39
Co—N—S/C-600	0.13	0.00	2.87	3.61
Co—N—S/C-700	0.15	0.02	4.80	3.76
Co—N—S/C-800	0.14	0.01	4.04	3.69
Co—N—S/C-900	0.11	−0.14	2.20	3.53
Co—N—S/C-1000	0.07	−0.17	1.06	3.43

[a] Electrode rotation rate: 1500 rpm.

As is well known, the ORR can proceed by two main routes: (i) direct 4-electron reduction to produce H_2O and (ii) less efficient 2-electron reduction to produce H_2O_2. To gain insight into the ORR mechanism quantitatively catalyzed by Co—N—S/C catalysts, RDE measurements were conducted for the best-performing catalyst, Co—N—S/C-700, at different electrode rotation rates from 300 to 2400 rpm; the results are shown in Fig. 7(a). The number of electrons transferred (n) was calculated on the basis of rotating disk electrode theory (the Koutecky-Levich theory). According to this theory, the disk current density (j) on an RDE can be expressed as follows:

$$\frac{1}{j} = \frac{1}{j_f} + \frac{1}{j_k} + \frac{1}{j_d} = \frac{1}{j_f} + \frac{1}{j_k} + \frac{1}{B\omega^{1/2}} \quad (1)$$

$$B = 0.2nFC_{O_2}D_{O_2}^{2/3}\nu^{-1/6} \quad (2)$$

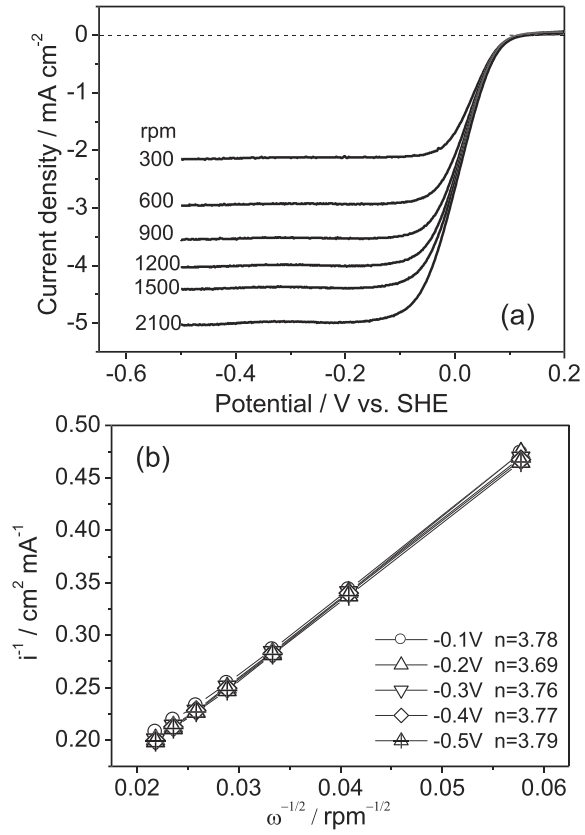

Fig. 7. (a) Rotating disk electrode measurements for oxygen reduction on Co—N—S/C-700 at a scan of 5 mV s^{-1} in O_2-saturated 0.1 M KOH solution; (b) K–L plots for Co—N—S/C-700, obtained from the data in (a).

where j is the total current density at a given electrode potential; j_f is the effect of Nafion ionomer inside the catalyst layer on the measured current density; j_k is the kinetic current density; j_d is the diffusion limiting current density; B is the Levich constant; ω is the electrode rotation rate (rpm); n is the number of electrons involved in the reaction; F is the Faraday constant (96485 C mol^{-1}); Do_2 and Co_2 are the diffusion coefficient of dissolved oxygen (cm^2 s^{-1}) and the concentration of dissolved oxygen (mol cm^{-3}), respectively; and ν is the kinematic viscosity of the electrolyte (cm^2 s^{-1}). A plot of $1/j$ against $\omega^{-1/2}$ can be used to determine the value of B. Fig. 7(b) shows Koutechy-Levich (K–L) plots for the ORR on Co–N–S/C-700 electrodes at four different electrode potentials (−0.40, −0.30, −0.20, and −0.10 V, respectively) from Fig. 7(a). The linearity of the K-L plots suggests first-order reaction kinetics toward the concentration of dissolved oxygen. In addition, the near parallelism of the fitting lines indicates similar electron transfer numbers for the ORR at different potentials. The electron transfer number was thus calculated from the slopes of the K–L plots to be an average of 3.77, suggesting that the catalyzed ORR is an approximate 4-electron transfer process of O_2 to water. Co-based catalysts generally tend to catalyze the ORR through a 2-electron pathway, producing H_2O_2, which is capable of oxidizing and splitting active sites [41,42]. Due to its chemical activity, H_2O_2 can corrode the carbon support, membrane, and ionomer, resulting in poor membrane electrode assembly stability. However, in the present work, 3.7 was achieved using salen as the nitrogen precursor, indicating that these catalysts could catalyze a 4-electron water production dominated ORR process rather than H_2O_2 production dominated one, which may be more favorite for fuel cell application.

To further verify the ORR catalytic pathways of the catalyst, the RRDE technique was used to quantitatively monitor the peroxide species formed during the ORR process. The hydrogen peroxide yield (%H_2O_2) and the electron number (n) during the ORR can be determined by the following equations [43]:

$$\%H_2O_2 = 100 \times \frac{2I_r/N}{I_d + I_r/N} \quad (3)$$

$$n = \frac{4I_d}{I_d + I_r/N} \quad (4)$$

where I_d is the disk current, I_r is the ring current, and $N = 0.37$ is the RRDE collection efficiency. Fig. 8 shows the n value and the corresponding percentage of H_2O_2 as a function of the applied electrode potential on the disk. As can be seen, the ORR electron number is decreased with negatively scanning the electrode potential. This may be explained by the fact that when the electrode potential becomes more negative, the reaction from $O_2 \rightarrow H_2O_2$ may become much faster than the reaction from $O_2 \rightarrow H_2O$, resulting in more H_2O_2. The number of electrons transferred was calculated to be 3.6–3.9 over the potential range of −0.05 ~ −0.60 V, which agrees very well with the value obtained from the K–L plots based on RDE measurements. Moreover, Fig. 8(b) also shows that 3.7–19.9% H_2O_2 is produced during the ORR process when using Co–N–S/C-700 catalyst. Thus, one can conclude that this catalyst mainly catalyzes an overall 4-electron transfer ORR process through a (2 + 2)-electron transfer pathway.

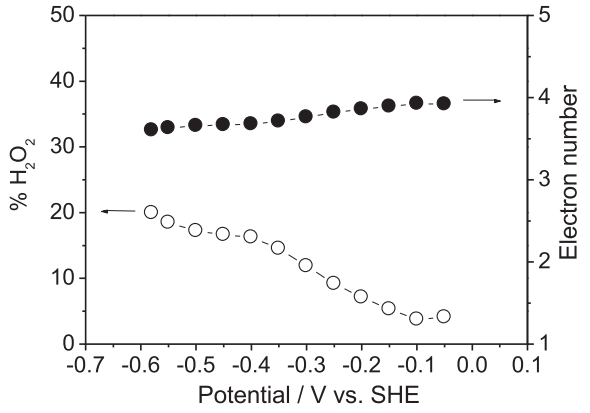

Fig. 8. (a) Rotating ring-disk electrode measurements for oxygen reduction on Co–N–S/C-700 at a scan of 5 mV s^{-1} in O_2-saturated 0.1 M KOH solution; (b) the corresponding percentage of H_2O_2 produced and electron transfer numbers of Co–N–S/C-700 at a rotation speed of 1600 rpm.

3.3. ORR catalyzed by Co–N–S/C catalysts in the presence of methanol (methanol tolerance)

Direct methanol fuel cells (DMFCs) have attracted considerable interest as potential alternative power sources for automobiles and portable electronics. However, one of their major challenges is methanol crossover from anode to cathode, which depresses ORR performance through directly reacting with the Pt-based electrocatalyst. Therefore, developing cathode ORR catalysts that have less or no catalytic activity toward methanol oxidation has been an important area in DMFC research. In the present work, the synthesized Co–N–S/C-700 catalyst was tested in the presence of methanol in an O_2-saturated electrolyte solution to assess their methanol tolerance. The results are presented in Fig. 9. For a good comparison, a similar set of ORR current–voltage curves catalyzed

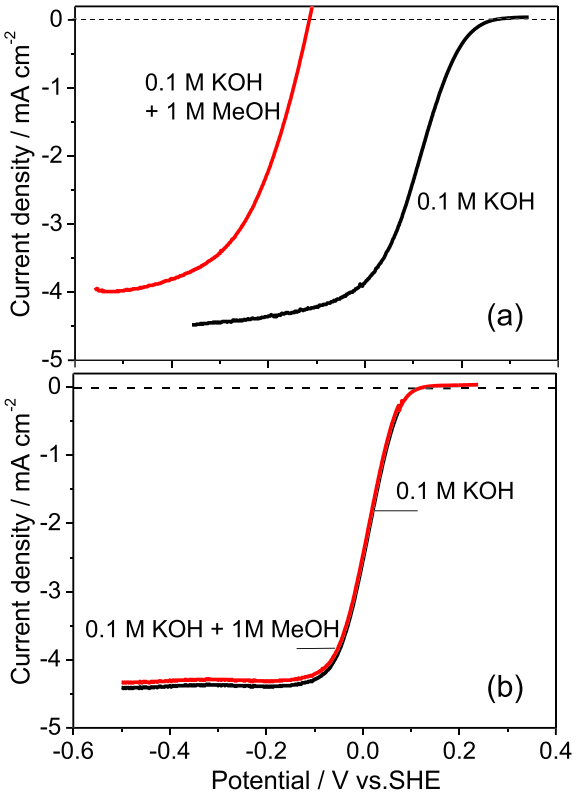

Fig. 9. Current–voltage curves for the ORR catalyzed by (a) Co–N–S/C-700 catalyst and (b) Pt/C catalyst, in O_2-saturated 0.1 M KOH electrolyte without and with 1.0 M methanol solution. Potential scan rate: 5 mV s^{-1}. Electrode rotation rate: 1500 rpm. Catalyst loading: 70.6 μg cm^{-2}.

by a commercially available Pt/C catalyst is also presented. Fig. 9(a) clearly shows that Pt/C suffers a dramatic loss in ORR catalytic activity when 1.0 M methanol is present in the solution. The half-wave potential of the ORR on Pt/C undergoes a negative shift of about 300 mV. This shift might be mainly caused by methanol oxidation producing a CO intermediate, which then adsorbs on and poisons the Pt active sites for the ORR. The result indicates that Pt/C has no methanol tolerance. However, when Co–N–S/C-700 catalyst was used in the same O_2-saturated electrolyte solution containing 1.0 M methanol, almost no changes were observed, as indicated by the ORR onset potential and current density as well as the half-wave potential, as shown in Fig. 9(b). Compared with Pt/C catalyst, the novel Co–N–S/C-700 catalyst has the unique advantage of selectivity toward the ORR, demonstrating perfect methanol tolerance.

4. Conclusions

A cost-effective chemical, salen, was used as a ligand to form carbon-supported Co-salen complex (Co-salen/C) by a simple solid–sate reaction. This complex was then heat treated at various temperatures to optimize its ORR activity. ORR test results in an O_2-saturated 0.1 M KOH solution showed that all of the resulting Co–N–S/C catalysts had strong catalytic activity toward the ORR, but the catalyst heat treated at 700 °C yielded the best ORR activity. ORR kinetic measurements and data analysis using the Koutecky–Levich theory and the RRDE technique revealed that the overall electron transfer number for the catalyzed ORR was in the range of 3.6–3.9, suggesting that the ORR catalyzed by Co–N–S/C catalysts is an approximate 4-electron process. Moreover, the Co–N–S/C-700 catalyst has no catalytic activity toward methanol oxidation, showing strong methanol tolerance. Therefore, Co–N–S/C-700 is expected to be a very promising cathodic catalyst for potential applications in both alkaline PEM fuel cells and DMFCs.

Acknowledgments

The authors gratefully acknowledge the financial support of the National Natural Science Foundation of China (21173039), the Specialized Research Fund for the Doctoral Program of Higher Education of China (20110075110001), the Innovation Program of the Shanghai Municipal Education Commission (14ZZ074) and the Fundamental Research Funds for the Central Universities (CUSF-DH-D-201450).

References

[1] W.B. Kim, T. Voitl, G.J. Rodriguez-Rivera, J.A. Dumesic, Science 305 (2004) 1280–1283.
[2] J.L. Fernández, D.A. Walsh, A.J. Bard, J. Am. Chem. Soc. 127 (2004) 357–365.
[3] E. Antolini, Energy Environ. Sci. 2 (2009) 15–31.
[4] A.E.S. Sleightholme, J.R. Varcoe, A.R. Kucernak, Electrochem. Commun. 10 (2008) 151–155.
[5] A. Morozan, B. Jousselme, S. Palacin, Energy Environ. Sci. 4 (2011) 1238–1254.
[6] J.R. Varcoe, R.C.T. Slade, G.L. Wright, Y. Chen, J. Phys. Chem. B 110 (2006) 21041–21049.
[7] C. Coutanceau, L. Demarconnay, C. Lamy, J.M. Léger, J. Power Sources 156 (2006) 14–19.
[8] Y.-J. Wang, J. Qiao, R. Baker, J. Zhang, Chem. Soc. Rev. 42 (2013) 5768–5787.
[9] R. Jasinski, Nature 201 (1964) 1212–1213.
[10] S. Gupta, D. Tryk, I. Bae, W. Aldred, E. Yeager, J. Appl. Electrochem. 19 (1989) 19–27.
[11] R. Bashyam, P. Zelenay, Nature 443 (2006) 63–66.
[12] K. Lee, L. Zhang, H. Lui, R. Hui, Z. Shi, J. Zhang, Electrochim. Acta 54 (2009) 4704–4711.
[13] V. Nallathambi, J.-W. Lee, S.P. Kumaraguru, G. Wu, J. Power Sources 183 (2008) 34–42.
[14] D.C. Higgins, J. Wu, W. Li, Z. Chen, Electrochim. Acta 59 (2012) 8–13.
[15] M. Lefèvre, E. Proietti, F. Jaouen, J.-P. Dodelet, Science 324 (2009) 71–74.
[16] C.W.B. Bezerra, L. Zhang, K. Lee, H. Liu, A.L.B. Marques, E.P. Marques, Electrochim. Acta 53 (2008) 4937–4951.
[17] F. Jaouen, E. Proietti, M. Lefevre, R. Chenitz, J.-P. Dodelet, G. Wu, Energy Environ. Sci. 4 (2011) 114–130.
[18] Z. Chen, D. Higgins, A. Yu, L. Zhang, J. Zhang, Energy Environ. Sci. 4 (2011) 3167–3192.
[19] J. Qiao, L. Xu, L. Ding, L. Zhang, R. Baker, X. Dai, J. Zhang, Appl. Catal. B-Environ. 125 (2012) 197–205.
[20] G. Faubert, G. Lalande, R. Côté, D. Guay, J.P. Dodelet, L.T. Weng, Electrochim. Acta 41 (1996) 1689–1701.
[21] T. Okada, M. Gokita, M. Yuasa, I. Sekine, J. Electrochem. Soc. 145 (1998) 815–822.
[22] G. Wu, H.T. Chung, M. Nelson, K. Artyushkova, K.L. More, C.M. Johnston, ECS Trans. 41 (2011) 1709–1717.
[23] A. Pacuła, K. Ikeda, T. Masuda, K. Uosaki, J. Power Sources 220 (2012) 20–30.
[24] R. Kothandaraman, V. Nallathambi, K. Artyushkova, S.C. Barton, Appl. Catal. B-Environ. 92 (2009) 209–216.
[25] Z. Chen, D. Higgins, H. Tao, R.S. Hsu, Z. Chen, J. Phys. Chem. C 113 (2009) 21008–21013.
[26] H.-J. Zhang, H.-C. Kong, X. Yuan, Q.-Z. Jiang, J. Yang, Z.-F. Ma, Int. J. Hydrogen Energy 37 (2012) 13219–13226.
[27] J.R. Pels, F. Kapteijn, J.A. Moulijn, Q. Zhu, K.M. Thomas, Carbon 33 (1995) 1641–1653.
[28] G. Liu, X. Li, J.-W. Lee, B.N. Popov, Catal. Sci. Technol. 1 (2011) 207–217.
[29] C.Z. Deng, M.J. Dignam, J. Electrochem. Soc. 145 (1998) 3507–3512.
[30] M. Yuasa, A. Yamaguchi, H. Itsuki, K. Tanaka, M. Yamamoto, K. Oyaizu, Chem. Mater. 17 (2005) 4278–4281.
[31] N.P. Subramanian, S.P. Kumaraguru, H. Colon-Mercado, H. Kim, B.N. Popov, T. Black, D.A. Chen, J. Power Sources 157 (2006) 56–63.
[32] L. Deng, M. Zhou, C. Liu, L. Liu, C. Liu, S. Dong, Talanta 81 (2010) 444–448.
[33] K. Sawai, N. Suzuki, J. Electrochem. Soc. 151 (2004) A682–A688.
[34] T.S. Olson, S. Pylypenko, J.E. Fulghum, P. Atanassov, J. Electrochem. Soc. 157 (2010) B54–B63.
[35] I. Alstrup, I. Chorkendorff, R. Candia, B.S. Clausen, H. Topsøe, J. Catal. 77 (1982) 397–409.
[36] T.K.T. Ninh, L. Massin, D. Laurenti, M. Vrinat, Appl. Catal. A-Gen. 407 (2011) 29–39.
[37] J.P. Boudou, J. Boulègue, L. Maléchaux, M. Nip, J.W. de Leeuw, J.J. Boon, Fuel 66 (1987) 1558–1569.
[38] M. Matsumoto, T. Miyazaki, S. Fujieda, A. Ishihara, K.-I. Ota, H. Imai, ECS Trans. 50 (2013) 1759–1767.
[39] S. Li, L. Zhang, H. Liu, M. Pan, L. Zan, J. Zhang, Electrochim. Acta 55 (2010) 4403–4411.
[40] C.W.B. Bezerra, L. Zhang, K. Lee, H. Liu, J. Zhang, Z. Shi, Electrochim. Acta 53 (2008) 7703–7710.
[41] H. Liu, C. Song, Y. Tang, J. Zhang, J. Zhang, Electrochim. Acta 52 (2007) 4532–4538.
[42] L. Zhang, J. Zhang, D.P. Wilkinson, H. Wang, J. Power Sources 156 (2006) 171–182.
[43] U.A. Paulus, T.J. Schmidt, H.A. Gasteiger, R.J. Behm, J. Electroanal. Chem. 495 (2001) 134–145.